Author(s): Pamuła, Małgorzata; Bulatov, Evgeny; Helttunen, Kaisa

Title: Binding of ion pairs and neutral guests by aryl-extended mesop-hydroxyphenyl calix[4]pyrrole : The interplay between three binding sites

Year: 2023

Version: Published version

Pamuła, M., Bulatov, E., & Helttunen, K. (2023). Binding of ion pairs and neutral guests by aryl-extended mesop-hydroxyphenyl calix[4]pyrrole : The interplay between three binding sites. Journal of Molecular Structure, 1273(5), Article 134268. https://doi.org/10.1016/j.molstruc.2022.134268

Journal of Molecular Structure 1273 (2023) 134268

Contents lists available at ScienceDirect

Journal of Molecular Structure

journal homepage: www.elsevier.com/locate/molstr

Binding of ion pairs and neutral guests by aryl-extended *meso–p*-hydroxyphenyl calix[4]pyrrole: The interplay between three binding sites

Małgorzata Pamuła, Evgeny Bulatov, Kaisa Helttunen*

Department of Chemistry, Nanoscience Center, University of Jyvaskyla, P.O. Box 35, FI-40014, Finland

ARTICLE INFO

Article history:
Received 8 August 2022
Revised 20 September 2022
Accepted 2 October 2022

Keywords:
Anions
Calix[4]pyrroles
Host-guest systems
Supramolecular chemistry
X-ray crystallography

ABSTRACT

An aryl-extended calix[4]pyrrole with four *meso–p*-hydroxyphenyl substituents was investigated as a host for chloride, acetate, and benzoate anions. Crystal structures of pyridinium and imidazolium chloride complexes were obtained in which chloride ions are hydrogen bonded *exo*-cavity to the upper rim hydroxyl groups, and the aromatic cations are bound to the shallow cavity of the host. Furthermore, the calix[4]pyrrole formed a hydrogen bonded dimeric capsule templated by inclusion of adiponitrile guest in the *endo*-cavity binding site. NMR titrations revealed the preference of the OH groups of the host to bind anionic guests in solution. Benzoate anion had the highest binding constant (4 700 M^{-1}) in acetonitrile. Density functional theory (DFT) calculations indicated that the *exo*-cavity complex with chloride anions was favoured by 23.2 kJ/mol over the *endo*-cavity complex, whereas the energies of *endo*- and *exo*-cavity benzoate complexes were of similar magnitude due to dispersion interactions between the host and the guest.

1. Introduction

Calix[4]pyrroles are known for their versatile ability to host neutral [1] and charged molecules [2]. Complexation of biologically important anions, such as halides [3], phosphates [4,5], and carboxylates[6] is enabled by four hydrogen bonds to the pyrrolic NH groups in the binding cavity. Simultaneously, convergent orientation of the pyrrole rings in cone conformation generates a shallow electron-rich cup under the anion binding site [7], which can attract cations in the solid state [8,9] and in solution leading to cascade complexation of ion pairs [10] and generation of supramolecular polymers [11].

The cavity of unsubstituted octamethylcalix[4]pyrrole has proper shape and size for binding small halide anions, particularly fluoride [12]. In addition, the anion binding properties can be modulated by functionalization of calix[4]pyrroles to increase affinity to larger anions, such as benzoate, which is important as a food and pharmaceutical preservative and in treatment of urea cycle enzyme disorders [13]. C-rim fluoro-substituted octamethyloctafluorocalix[4]pyrrole shows higher binding affinities towards Cl^-, $H_2PO_4^-$, acetate and benzoate in comparison to the parent receptor, octamethylcalix[4]pyrrole [14–16]. A higher order decafluorocalix[5]pyrrole forms an acetate complex in the solid state stabilized by five hydrogen bonds involving the acetate guest, pyrrolic NH groups and a bridging water molecule [16]. Expanded calix[2]benzo[4]pyrroles also show increased affinity towards larger anions, including acetate, both X-ray diffraction and NMR studies indicating that an acetate anion binds within the receptor cavity [17]. Furthermore, covalently connecting two calix[4]pyroles into a homodimer have proven to be an efficient method to enhance the binding of isophthalate anion [18].

Substitution of the *meso*–carbons with aromatic groups in the same relative position generates so called two-wall α,α and four-wall $\alpha,\alpha,\alpha,\alpha$ aryl-extended calix[4]pyrroles with deep polar cavities [19]. The deep cavity readily forms *endo*-complexes with neutral polar guests, such as pyridine *N*-oxides in water[20] and in organic solvents [21], and encapsulates DMF in the solid state [22]. Recently, pyrazine *N,N'*-dioxide has been shown to interact both with the electron-poor and electron-rich cavities of aryl-extended calix[4]pyrroles forming guest mediated hydrogen bonding networks and capsules [23]. In addition, *endo*-complexation of anions into the deep cavity has been achieved with bis-(nitrophenyl)–

* Corresponding author.
E-mail address: kaisa.j.helttunen@jyu.fi (K. Helttunen).

https://doi.org/10.1016/j.molstruc.2022.134268

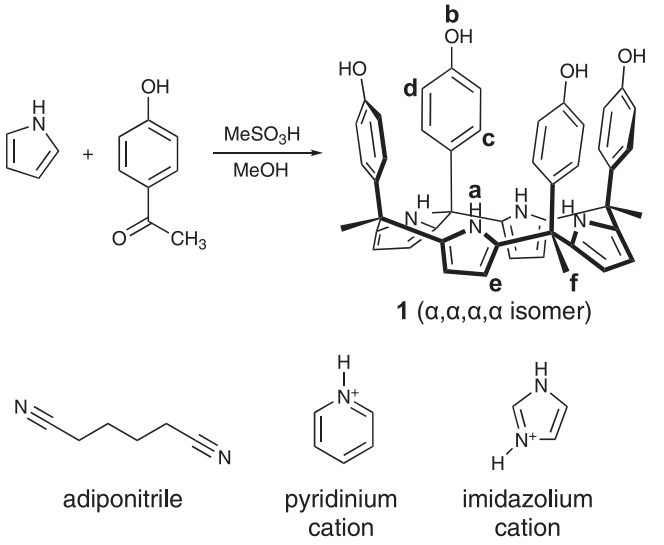

Scheme 1. Synthesis of *meso-p*-hydroxyphenyl calix[4]pyrrole **1**, and cationic and neutral guests used in the crystal structures.

meso-substituted calix[4]pyrroles with nitrate [24], acetate, dihydrogenphosphate and hydrogen carbonate [25].

Four-wall aryl-extended *meso–p*-hydroxyphenyl calix[4]pyrrole (**1**, Scheme 1) [19,22] features three different binding sites: a deep aromatic cavity containing a converging array of NH groups for *endo*-binding, the upper rim OH groups for *exo*-complexation as well as the shallow electron rich cavity. These features afford **1** a versatile supramolecular host for crystal engineering purposes, as indicated by several crystal structures deposited into the Cambridge structural database (CSD) [26]. Ethanol [19], acetonitrile [27], dimethylformamide [22] and pyrazine *N*-oxide [23] have formed inclusion complexes within the deep cavity of **1**, while the crystal packing displays hydrogen bonding mediated chains between the upper rim hydroxyl groups. In addition, crystal structures with fluoride (CSD Refcode GUGQOO) [19] and chloride (POCCIU) [28] salts show *exo*-cavity binding of the halides via hydrogen bonds to the upper rim hydroxyls generating anion mediated one-dimensional chains. Therefore, the tendency to form hydrogen bonded chains via rim-to-rim assembly is dominating, apart from acetic acid solvate packing into hydrogen bonded trimers [22]. The role of the cation is significant in the assembly in the second dimension: a methyl group of a tetramethylammonium fits to the shallow cavity and the cation connects the calix[4]pyrroles into a two-dimensional supramolecular network, whereas only part of a bulkier tetrabutylammonium cation interacts with the shallow cavity leading to less regular packing. However, the selection of cations to induce regular packing has been limited to tetramethylammonium, while potassium and caesium afford good complementarity with a single shallow cavity. Complexes of pyridinium and imidazolium derivatives are relatively rare and most studies are limited to unsubstituted octamethylcalix[4]pyrroles and to bulkier *N*-alkylated derivatives used in ionic liquids [8,9,29] which do not allow as regular assemblies. To the best of our knowledge, only one crystal structure where pyridinium has been included in the shallow cavity of an aryl extended calix[4]pyrrole-based metal-organic cage (IDOKIY) [30] is known and no imidazolium complexes were found from the CSD database.

Herein, we report new crystal forms of aryl-extended calix[4]pyrrole **1** with pyridine and imidazole hydrochloride, as well as NMR titration experiments and DFT calculations with chloride, acetate, and benzoate anions to investigate the interplay of the three different binding sites. As the formation of offset face-to-face hydrogen bonded dimeric units of **1** with the inclusion of acetonitrile molecules in the cavity was observed, ditopic adiponitrile guest was used to crystallize dimeric capsules. These results show that all three binding sites can be utilized in design of various supramolecular architectures based on **1**.

2. Materials and methods

2.1. General

All solvents and chemicals were purchased from commercial sources and used without further purification unless otherwise stated.

2.2. Synthesis of 1

4-Hydroxyacetophenone (2.61 g, 19.0 mmol) and freshly distilled pyrrole (1.33 ml, 19.0 mmol) were dissolved in dry methanol (56 ml) under nitrogen atmosphere. Methanesulfonic acid (0.6 ml, 9.2 mmol) was added dropwise within 5 min. The reaction mixture was stirred at room temperature and the progress of the reaction was followed by TLC (8% methanol/CH_2Cl_2). After approximately 24 h the reaction mixture was quenched with triethylamine (1.28 ml). The resulting mixture was diluted with chloroform (56 ml) and passed through a pre-column using chloroform/methanol (1:1) eluent to remove polymeric by-products. After evaporation of the solvent, the crude was recrystallized from glacial acetic acid (23 ml, approx. 1 ml/145 mg of crude) and the formed orange precipitate was filtered and dried under vacuum overnight. Recrystallization from ethanol/water (21% v/v H_2O in ethanol; 19 ml) afforded light yellow crystals, which were filtered and dried under vacuum (yield 0.33 g, 9.3%, R_f = 0.14 silica gel, 8% methanol in CH_2Cl_2). Alternatively, **1** was obtained as a pyridinium complex **1a** when the reaction was quenched with pyridine and purified as mentioned above. The NMR and MS spectra corresponded to literature [19]. ^{1}H NMR (500 MHz, [D_3]acetonitrile): δ 7.89 (br t, 4H, NH), 6.83 (br s, 4H, OH), 6.78–6.73 (m, 8H), 6.70–6.65 (m, 8H), 5.99 (d, J = 2.6 Hz, 8H), 1.82 (s, 12H, CH_3) ppm.

2.3. NMR measurements

NMR spectra were recorded with a Bruker Avance III 500 spectrometer equipped with a Prodigy cryoprobe. The NMR titrations were performed at a constant concentration of the host (1 mM) in [D_3]acetonitrile. The chemical shifts were referenced to the residual solvent signal of acetonitrile (1.94 ppm). The NMR data were analysed, and the figures were prepared with Mnova software version 14.2.1 (Mestrelab Research, S.L.). The binding constants were calculated by fitting the obtained NMR data to a theoretical 1:1 binding isotherm using HypNMR2008 software [31].

2.4. Single crystal X-ray diffraction

Single crystals of the complexes were grown from slow diffusion of acetonitrile vapours into a concentrated solution of **1** and the corresponding guest in ethanol or methanol. The obtained crystals were immersed in cryo-oil, mounted in a MiTeGen loop and measured at 120 K on a Rigaku Oxford Diffraction Supernova diffractometer using CuK_α irradiation (λ = 1.54184 Å). CrysAlisPro program (CrysAlisPro 1.171.38.41, Rigaku Oxford Diffraction, 2015) was used for the unit cell refinement, absorption correction (gaussian or analytical) and data reduction. Using OLEX2 graphical interface [32], structure solution was performed using SHELXT [33] (intrinsic phasing method) or Superflip [34–36] (charge flipping method) programs, and structure refinement on F^2 was performed using SHELXL [37] program. Hydrogen

atoms were calculated in idealized positions and refined as riding atoms with constrained parameters U_{iso}= 1.2–1.5·U_{eq} (parent atom). The pyridinium and imidazolium cations in structures **1a** and **1b**, respectively, were modelled as disordered over two positions related by symmetry with occupancies fixed to 0.5 for each position and rigid bond restraints were applied. The figures were prepared using OLEX2 [32]. CCDC 2175934-2175936 contains the supplementary crystallographic data for this paper.

2.5. DFT calculations

The calculations were carried out using Gaussian 09 program revision E.01 [38]. The geometry optimizations were performed using density functional theory (DFT) with B3LYP functional [39,40], 6-311++G(d,p) basis set [41–44] and GD3 dispersion correction [45] both in gas phase and in solution. The polarized continuum model (PCM) was used to study the influence of the acetonitrile solvent. For all the optimized structures, frequency calculations were conducted to ensure optimization to the local energy minima. The initial coordinates of *exo*-Cl complex were obtained from the crystal structure **1a** and the anion position was modified accordingly with Maestro program [46]. Structures were analysed and figures were prepared with Maestro and Mercury [47] software. Cambridge Structural Database version 5.43 was used to search average hydrogen bond distances (mean of the bond length distribution).

3. Results and discussion

3.1. Synthesis and crystal structures

Synthesis of aryl-extended *meso*–*p*-hydroxyphenyl calix[4]pyrrole **1** (Scheme 1) was achieved by condensation of pyrrole and *p*-hydroxyacetophenone catalyzed by methanesulfonic acid according to modified literature protocols [19,22]. The desired $\alpha,\alpha,\alpha,\alpha$ isomer was separated by crystallization from glacial acetic acid, followed by recrystallization from ethanol/water at 9.3% yield. Single crystals of **1** with pyridine hydrochloride were obtained by dissolving the host and the guest in ethanol at 2:1 ratio, where crystals grew under acetonitrile vapour diffusion. Cocrystal **1a** (Fig. 1) contains two molecules of **1** per a molecule of pyridinium chloride and five molecules of acetonitrile, one of them being disordered over two sites. The acetonitrile molecule inside a deep cavity formed by four *meso*–*p*-hydroxyphenyl substituents in axial orientation is hydrogen bonded to the pyrrolic NH groups. Two of the upper rim hydroxyl groups are involved in hydrogen bonding interactions with the chloride anion (O···Cl 3.14–3.20 Å) in *exo*-cavity binding, and two hydroxyl groups form hydrogen bonding interactions with the second calix[4]pyrrole (O···O 2.75–2.83 Å). Two more hydrogen bonds connect the chloride anion to another calix[4]pyrrole generating anion mediated hydrogen bonded chains. In addition, a pyridinium cation was found sandwiched between the shallow, electron-rich cavities of the calix[4]pyrrole molecules, which links the hydrogen bonded chains into cation-mediated two-dimensional sheets (Fig. 2) similarly to the previously discovered tetramethylammonium chloride complex [28]. The pyridinium cation appears slightly larger than the cavity, generating a gap between the β-pyrrolic protons where two acetonitrile molecules form short contacts with the *meso*–methyl groups of **1**.

The crystal structure **1a** contains three symmetrically non-equivalent molecules of **1** and two symmetrically inequivalent pyridinium chlorides (Fig. S8). Two of the non-equivalent hosts and the second pyridinium chloride form the second type of sheet packing which differs mainly by the orientation of the pyridinium cation and acetonitrile molecules near the lower rim interface (Fig. S9).

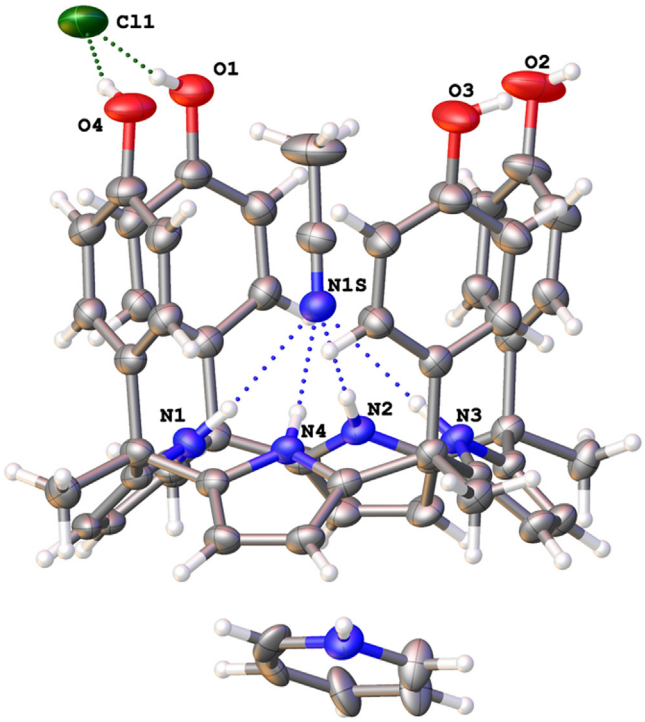

Fig. 1. One of the three molecules of **1** in the crystal structure of **1a**. Acetonitrile molecules outside of the deep cavity are omitted for clarity.

Since crystal structures of bromide complexes of **1** are not known, co-crystallizations with pyridinium bromide were attempted using variations of the same crystallization method. The obtained crystals were not of sufficient quality to complete the refinement but nevertheless, an isostructural packing and hydrogen bonding network as in **1a** with a bromide anion connecting the adjacent calix[4]pyrroles were visible indicating that pyridine hydrochloride and hydrobromide salts are readily complexed by **1** in the solid state.

Next, encapsulation of a smaller aromatic ammonium cation was pursued by crystallization of **1** with imidazole hydrochloride yielding structure **1b** with the host and the guest at the expected 2:1 stoichiometry. The structure contains single acetonitrile molecule hydrogen bonded to the NH groups in the deep aromatic cavity (Fig. 3). The hydrogen bonding network in **1b** is similar as in **1a** with O···O distances of 2.75–2.78 Å between the calix[4]pyrroles and O···Cl distances of 3.10–3.17 Å with the anion. The imidazolium cation is sandwiched between two shallow cavities (Fig. 4). In this case, the matching size of the imidazolium allows the cavities to face each other in a parallel alignment with a smaller distance than in **1a** (Fig. S10). After successfully finding a good match for the shallow cavity, complexation of a larger aromatic cation, adenine hydrochloride was also attempted from methanol and acetonitrile. Unfortunately, desired co-crystals were not obtained, since only host crystallized as a previously known acetonitrile solvate [27].

Structures **1a** and **1b** confirmed the expectation that **1** prefers to form hydrogen bonded or anion-mediated chains at the upper rim interface. On the other hand, acetonitrile seemed very good fit for the deep cavity. Ditopic guests, such as dicarboxylates [48,49] and bi-pyridine bis-*N*-oxide [50,51] are known to be good templates for calix[4]pyrrole dimers, even though this strategy has not been used for calix[4]pyrrole **1**. In the anion-mediated chains of **1a** and **1b**, the two directly hydro-

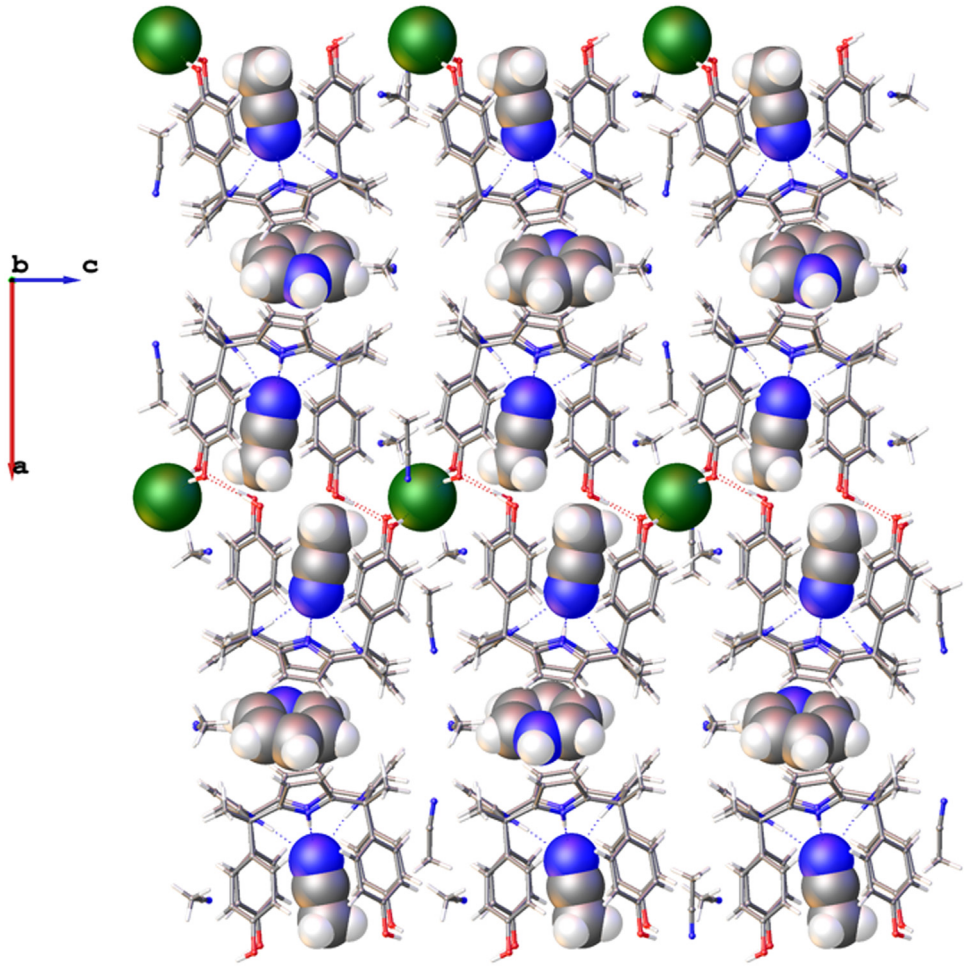

Fig. 2. Packing of a two-dimensional sheet in the crystal structure **1a** viewed along the b-axis. Atom colours: blue = nitrogen, green = chlorine, grey = carbon, red = oxygen, white = hydrogen.

gen bonded calix[4]pyrroles form an offset dimeric unit where the distance between the two acetonitrile nitrogens is 8.34–8.44 Å. This distance corresponds to a fully extended all *anti* conformation of adiponitrile, which contains four methylene units between the terminal nitrile groups. Therefore, this guest was used in the co-crystallization at 1:15 host:guest ratio from ethanol solution of **1** with acetonitrile vapour diffusion providing colourless block crystals (structure **1c**, Fig. 5). The crystal structure contains the desired dimeric hydrogen bonded capsule, which hosts an adiponitrile molecule hydrogen bonded to four pyrrole NH groups in each end (N···N 3.18–3.35 Å). The hydrogen bond distances span over a slightly longer range than in **1a** and **1b** with acetonitrile (3.17–3.25 Å). On the other hand, the distance between the adiponitrile nitrogens N1A and N2A is 8.39 Å as expected for a good fit in the capsule. The two hemispheres of the capsule are connected with three direct hydrogen bonds between the upper rim hydroxyl groups (O···O 2.69–2.76 Å), and by six water and ethanol mediated hydrogen bonds. The hydrogen bonding belt is continued via a bridging water molecule to the second dimeric capsule, which packs side by side in the crystal (Fig. S12). This assembly is completed by hydrogen bonds to the nitrile groups of three adiponitrile molecules located outside the deep cavity. Two of the *exo*-cavity adiponitriles also occupy the shallow cavities of the calix[4]pyrroles with their alpha and beta methylene groups adopting a *gauche* conformation to improve the fit with the cavity.

3.2. Binding studies

To evaluate how receptor **1** interacts with chloride anions in solution, ^{1}H NMR titrations were carried out in [D_3]acetonitrile, since it dissolves the host and tetrabutylammonium salts well and allows comparison of the binding behaviour with the solid-state studies. However, interactions between the bulky tetrabutylammonium cation and the shallow cavity were not expected in this polar aprotic solvent. The scope of the anions in the binding studies was expanded with acetate and benzoate due to their biological significance and lack of crystal structures with four-wall calix[4]pyrroles.

The ^{1}H NMR spectrum of **1** in [D_3]acetonitrile showed a broad resonance for NH at 7.89 ppm (a), another broad resonance for OH at 6.83 ppm (b), two signals at 6.75 and 6.68 ppm for the phenyl protons (c,d), and a doublet at 5.99 ppm for the β-pyrrolic protons (e) in the aromatic region. Addition of incremental amounts of tetrabutylammonium chloride to a millimolar solution of **1** in [D_3]acetonitrile led to a significant 2.2 ppm downfield shift of OH protons, which typically occurs upon the hydrogen bonding interactions with chloride anions (Fig. 6a). Additionally, the resonances corresponding to the CH protons of the phenol groups got closer towards each other and overlapped at about 0.2 eq. At 0.7 molar equivalents the aromatic protons emerged as two signals, signal d *orto* to the OH group shifting more. In contrast, NH protons and β-pyrrolic protons experienced only small chemical shift changes upon addition of 12 equivalents of the guest indicating that the

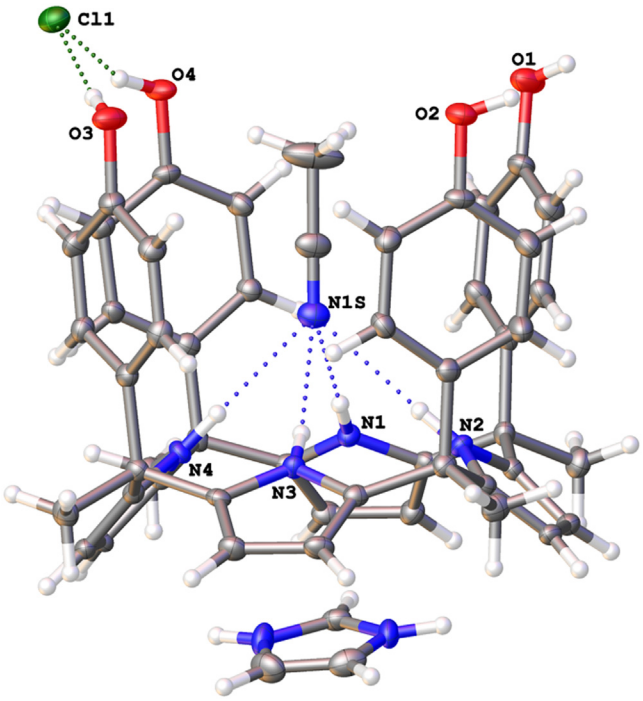

Fig. 3. Asymmetric unit in the crystal structure of **1b**.

Table 1
Binding constants and complexation induced shifts for **1** with tetrabutylammonium salts in [D_3]acetonitrile at 30 °C.

Anion	K (M^{-1})[a]	$\Delta\delta_{NH}$ (ppm)[b]	$\Delta\delta_{OH}$ (ppm)[b]
Cl^-	2 200	−0.04	2.30
CH_3COO^-	3 500	0.10	N.D.[c]
$C_6H_5COO^-$	4 700	0.08	5.12

[a] Errors < 15%.
[b] Extrapolated to 100% complex.
[c] Broadened beyond detection.

calix[4]pyrrole remains in a cone conformation with an acetonitrile molecule occupying the aromatic cavity as observed in the crystal structures. This finding is in agreement with the previous observations that aryl-extended calix[4]pyrroles with electron donating substituents provide repulsive anion···π interactions with halides [52]. We fitted the data to a theoretical 1:1 binding isotherm and obtained an apparent binding constant $K = 2\ 200\ M^{-1}$ from the fit (Table 1). Implementing higher order complexes, such as 1:2 or 2:1 did not improve the fit, indicating that 1:1 complex is the main species obtained at this range of concentrations.

Next, we performed an analogous titration with tetrabutylammonium acetate. In this case, the NH protons moved slightly downfield during titration (0.1 ppm) suggesting that they are involved with hydrogen bonding interactions with the guest, albeit to a small extent. Contrary, OH protons broadened beyond detec-

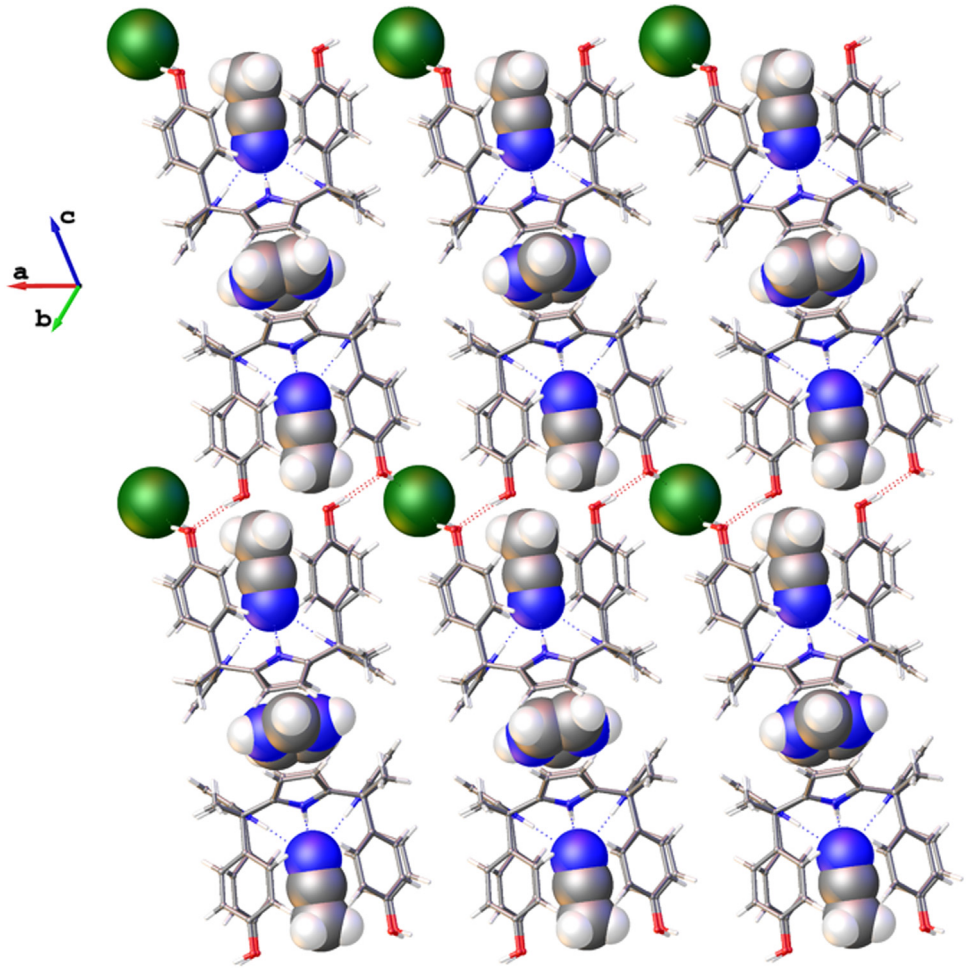

Fig. 4. Packing of a two-dimensional sheet in the crystal structure **1b** viewed along the a-axis. Atom colours: blue = nitrogen, green = chlorine, grey = carbon, red = oxygen, white = hydrogen.

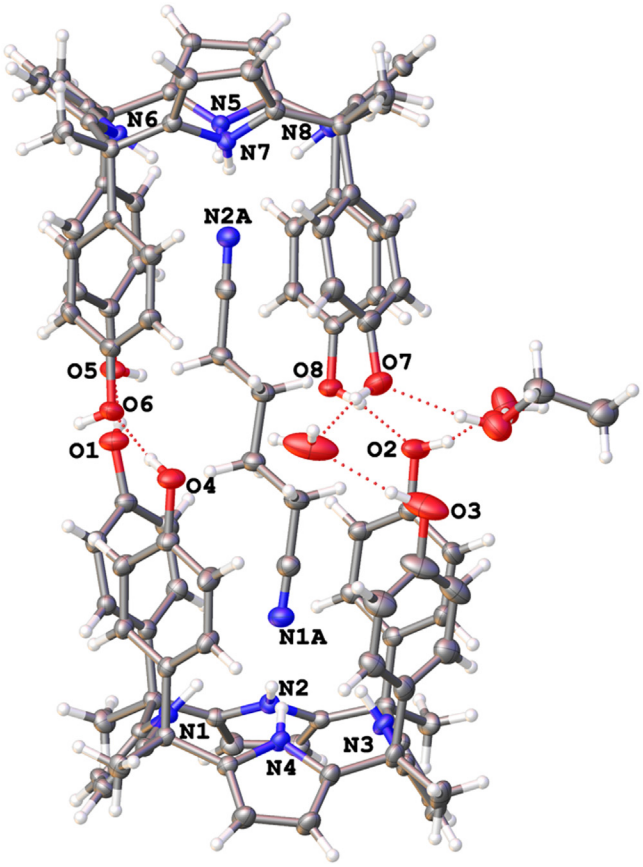

Fig. 5. Crystal structure **1c** showing hydrogen bonded capsule with inclusion of adiponitrile.

tion which was assigned as the protons being involved in an exchange process that was intermediate on the NMR timescale. In addition, the aryl c and d protons crossed as observed in titration with chloride, but this time d proton moved significantly less downfield. The apparent binding constant from the fit was 3500 M^{-1} for a 1:1 complex.

In an attempt to utilize $\pi\cdots\pi$ interactions provided by the meso–aryl walls in anion binding, NMR titration was performed with benzoate anion in similar conditions (Fig. 6b). After the addition of 0.1 molar equivalent of TBAOBz the peak corresponding to OH protons broadened again significantly, suggesting that the benzoate anion interacts with them in *exo*-cavity complex close to the NMR timescale. However, at 4.3 eq. of added guest sharpening of the signal allowed the analysis of the complexation induced shift, which was a significant 5.12 ppm suggesting strong hydrogen bonding interactions. The NH protons moved slightly downfield during titration similarly to the acetate titration. Saturation of the chemical shift changes was observed at six equivalents of the added guest and the resulting binding constant for 1:1 complex was found to be slightly larger than for chloride or acetate (4 700 M^{-1}).

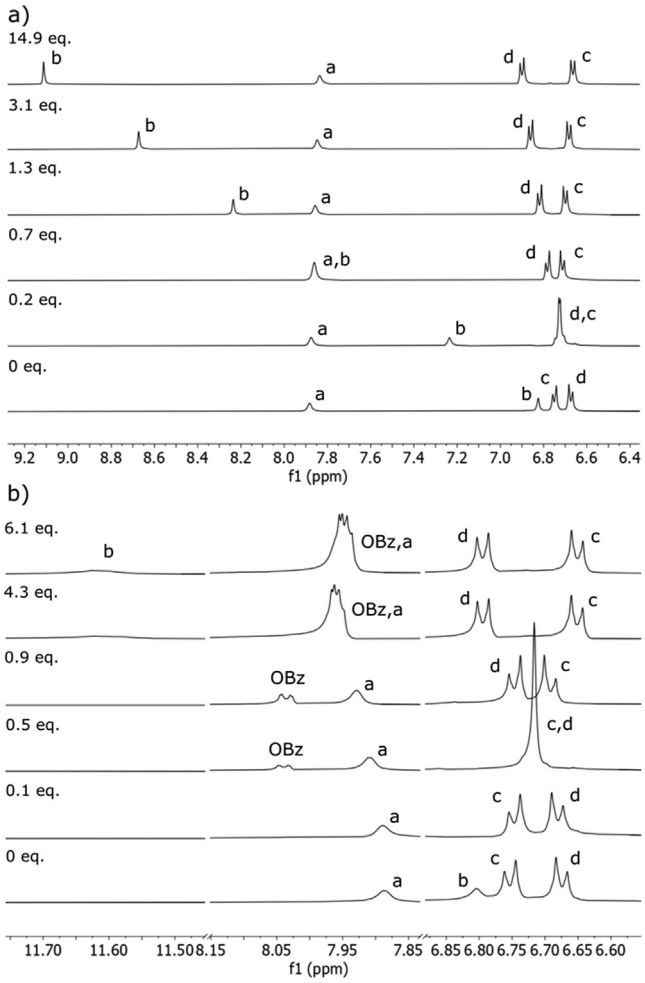

Fig. 6. The NMR titration of **1** (1 mM) with tetrabutylammonium a) chloride and b) benzoate in [D_3]acetonitrile. The amount of the added guest is shown as molar equivalents.

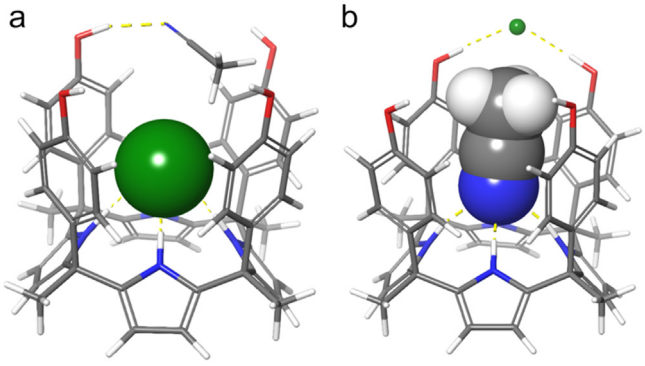

Fig. 7. DFT optimized structures a) *endo*-Cl and b) *exo*-Cl with implemented solvent model.

3.3. DFT calculations

Density functional theory calculations were performed in order to investigate how the position of chloride, acetate and benzoate within the host affect the geometry and relative energies of the anion complexes in solution. Two different complex models were taken into consideration (Fig. 7). The first model assumes that anions bind within the host cavity whereas an acetonitrile molecule forms a hydrogen bond with *p*–hydroxyl groups of the phenyl substituents (*endo*-Cl, *endo*-OAc, *endo*-OBz). In the second model anions form hydrogen bonds with two *p*–hydroxyl groups and an acetonitrile molecule is the one residing in the host cavity (*exo*-Cl, *exo*-OAc, *exo*-OBz). Calculations were performed in the gas phase and with implicit solvent model for acetonitrile.

In the *exo*-Cl complex in the gas phase the anion binds with two O–H···Cl^- hydrogen bonds, which are slightly elongated when the solvent effect is included. The O···Cl distances of 3.14 Å in solvent are very similar with the corresponding distances in the X-

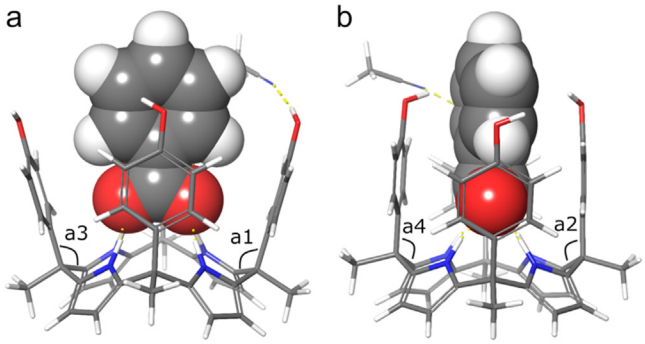

Fig. 8. DFT optimized structure of *endo*-OBz complex with implemented solvent model showing a) side view of the phenyl rings adopting wide angles a1 and a3, b) side view of the phenyl rings resting at narrow angles a2 and a4.

ray structures **1a** and **1b** (3.10–3.20 Å). In *exo*-carboxylate systems with the solvent effect the O–H···O bond lengths are very close to those in the gas phase. The O···O distances in *exo*-OAc and *exo*-OBz are within 2.61–2.64 Å, which is close to a typical hydrogen bond length in CSD between carboxylate groups and phenolic hydroxyls (2.62 Å). Similarly, the hydrogen bond distances from the pyrrolic NH groups to the acetonitrile (3.16–3.21 Å) in all calculated solvent structures show an excellent match with the N···N distances in **1a** and **1b**.

When chloride binds to the deep cavity with four hydrogen bonds to the pyrrolic NH groups, the hydrogen bond distances are 3.29 Å in *endo*-Cl, which is the most typical N···Cl^- distance in the CSD. The *endo*-OAc and *endo*-OBz have altogether four hydrogen bonds formed between the anion and the NH groups, two for each oxygen atom with bond lengths of 2.82–2.85 Å. The structures were compared with the crystal structures of terephthalate complexes with two-wall aryl-extended calix[4]pyrroles (LOMZUJ [25], PEYYOK, PEYYUQ and PEYZIF [53]), which show similar binding mode and hydrogen bond distances with the carboxylate group.

To compare the change in host conformation of the investigated complexes in both gas phase and in solution, four angles were determined between a mean plane defined by four pyrrolic nitrogen atoms and a plane consisting of the phenyl ring of each aromatic wall (Table S9, Fig. S15). For *endo*-OBz complex in the gas phase, angle a1 is slightly enlarged with respect to the *endo*-Cl and *endo*-OAc structures from 100° to 103°. While two interplanar angles a2 and a4 of the opposite phenol rings are opened beyond 95° for the acetate, the two phenyl substituents rest at a narrower 87–89° angle when the benzoate binds within the calix[4]pyrrole cavity (Fig. 8). Differently, the *exo*-carboxylate structures exhibit very similar geometry with each other while the aromatic walls are more opened upon chloride complexation. With carboxylates bound to the hydroxyl groups, adding solvent effect does not induce significant geometrical changes. Conversely, the *exo*-Cl structure experiences a small geometrical change as indicated by enlarged interplanar angles simultaneously with the increasing OH···Cl bond lengths. Overall, in all *endo*-structures, the calix[4]pyrrole adopts a distorted cone conformation where the interplanar angles are much larger when compared with the *exo*-variant of the complex affording a more open cavity. Opening of the aromatic walls is likely induced mainly by the carboxylate···π and Cl···π repulsion upon anion inclusion in the aromatic cavity.

The relative energies of *endo*- and *exo*-cavity complexes of **1** with chloride, acetate, and benzoate anions are shown in Table 2. The calculated energy values in gas phase increased for all models with bound anion in the cavity in comparison to the corresponding *exo*-cavity complexes indicating a lower stability of the *endo* variants. The energy difference between *endo*- and *exo*-cavity

Table 2
The energy differences between the *endo*- and *exo*-complexes $\Delta E = E_{endo} - E_{exo}$ in kJ·mol^{-1} calculated at B3LYP/6–311++G^{**} level.

	Cl^-	CH_3COO^-	$C_6H_5COO^-$
ΔE_{gp} [a]	18.3	61.7	4.5
ΔE_{sol} [b]	23.2	39.4	5.0

[a] In gas phase.
[b] With implicit solvent model for acetonitrile.

complexes is significantly higher for acetate in contrast to benzoate complexes by 57.2 kJ/mol in gas phase ($\Delta\Delta E_{gp}$) and by 34.4 kJ/mol in solution ($\Delta\Delta E_{sol}$). The energy difference between *endo*-Cl and *exo*-Cl increased slightly in solution giving ΔE_{sol} = 23.2 kJ/mol whereas for the acetate complexes ΔE_{sol} was slightly lower than ΔE_{gp}. In the benzoate structures, attractive dispersive interactions established between the benzene ring and the phenyl units of the aromatic wall (Fig. 8) increase complex stability suggesting that the energy gain caused by their formation overcomes the energy loss associated with distortion in the calix[4]pyrrole conformation and carboxylate···π repulsion. This is reflected in the ΔE_{gp} and ΔE_{sol} values that for benzoate binding turned out to be only 5 kJ/mol. Amongst all, the *exo*-complexes of **1** are predicted to be the most stable whereas the presence of the anion in a cavity leads to decrease in thermodynamic stability of the complex. Thus, the obtained computational results are in agreement with the experimental observation of downfield shifting of the hydroxyl protons in NMR titrations, as well as, with typical hydrogen bond lengths found in crystal structures.

4. Conclusion

The interactions of *endo*-, *exo*- and shallow cavity binding sites of *meso*–*p*-hydroxyphenyl calix[4]pyrrole **1** with ionic and polar guests were investigated in the solid state and in a polar non-protic solvent. The hydroxyl groups at the upper rim of the receptor form hydrogen bonds with adjacent hosts and anionic guests leading to crystallization of an anion-mediated hydrogen bonding chain at the upper rim. The shallow cavity readily attracts cations in the solid state, both pyridinium and imidazolium being sandwiched between two hosts. Interestingly, imidazolium was small enough to get symmetrically encapsulated, whereas in pyridine hydrochloride complex as in the previously investigated tetramethylammonium chloride complex, solvent molecules formed interactions with the cation through a gap between the lower rims of the hosts. In the solid state, an acetonitrile occupied the *endo*-binding site, and a long ditopic nitrile guest, adiponitrile was used to template crystallization of a dimeric hydrogen bonded capsule.

NMR titrations in acetonitrile indicated that anions preferentially bind with the OH groups rather than NH groups in agreement with the crystal structures. At a millimolar host concentration, 1:1 complexes were mainly observed and the highest binding constant was obtained for benzoate showing twofold increase over chloride. Optimized geometries and relative energies of the 1:1 *endo*- and *exo*-cavity anion complexes were determined from DFT calculations showing that the anions establish two hydrogen bonds with the OH groups in this binding mode. The *exo*-cavity complexes gave lower relative energies than the corresponding *endo*-cavity complexes in the order of $AcO^- > Cl^- > BzO^-$. The structure of the *endo*-OBz indicated dispersive interactions between the calix[4]pyrrole walls and benzoate, which stabilized the *endo*-cavity complex.

Overall, host **1** is a versatile building block for crystal engineering and supramolecular host-guest complexation utilizing efficiently all three binding sites. The trends of *exo*-cavity binding of anions with simultaneous inclusion of polar neutral guest was

also conveyed in solution and in the computational studies. Notably, the favourable interactions with aliphatic nitriles can be used to overcome the strong preference of rim-to-rim hydrogen bonding chains in this host to generate new dimeric capsule in the solid state, adding a new guest species for templating calix[4]pyrroles capsules.

Declaration of Competing Interest

The authors declare that they have no known competing financial interests or personal relationships that could have appeared to influence the work reported in this paper.

CRediT authorship contribution statement

Małgorzata Pamuła: Validation, Formal analysis, Investigation, Writing – original draft, Visualization. **Evgeny Bulatov:** Validation, Formal analysis, Investigation, Writing – review & editing, Visualization, Supervision. **Kaisa Helttunen:** Conceptualization, Writing – original draft, Writing – review & editing, Supervision, Project administration, Funding acquisition.

Data availability

Data will be made available on request.

Acknowledgements

We thank Dr. Laura Laverdure for help with computational part of our work. This work was supported by Academy of Finland (grants 309910, 314287, 335685).

Supplementary materials

Supplementary material associated with this article can be found, in the online version, at doi:10.1016/j.molstruc.2022.134268.

References

[1] W.E. Allen, P.A. Gale, C.T. Brown, V.M. Lynch, J.L. Sessler, Binding of neutral substrates by Calix[4]pyrroles, J. Am. Chem. Soc. 118 (1996) 12471–12472, doi:10.1021/ja9632217.
[2] I. Saha, J.T. Lee, C.-.H. Lee, Recent advancements in Calix[4]pyrrole-based anion-receptor chemistry, Eur. J. Org. Chem. (2015) 3859–3885, doi:10.1002/ejoc.201403701.
[3] P.A. Gale, J.L. Sessler, V. Král, Calixpyrroles, Chem. Commun. (1998) 1–8, doi:10.1039/a706280j.
[4] S.P. Mahanta, B.S. Kumar, P.K. Panda, Meso-diacylated calix[4]pyrrole: structural diversities and enhanced binding towards dihydrogenphosphate ion, Chem. Commun. 47 (2011) 4496–4498, doi:10.1039/c1cc10284b.
[5] A.F. Danil de Namor, M. Shehab, Recognition of biologically and environmentally important phosphate anions by calix[4]pyrrole: thermodynamic aspects, J. Phys. Chem. A. 108 (2004) 7324–7330, doi:10.1021/jp031343x.
[6] R. Nishiyabu, P. Anzenbacher, Sensing of antipyretic carboxylates by simple chromogenic calix[4]pyrroles, J. Am. Chem. Soc. 127 (2005) 8270–8271, doi:10.1021/ja051421p.
[7] S.K. Kim, J.L. Sessler, Calix[4]pyrrole-based ion pair receptors, Acc. Chem. Res. 47 (2014) 2525–2536, doi:10.1021/ar500157a.
[8] G.W. Bates, P.A. Gale, M.E. Light, Ionic liquid-calix[4]pyrrole complexes: pyridinium inclusion in the calixpyrrole cup, CrystEngComm 8 (2006) 300–302, doi:10.1039/b600251j.
[9] R. Custelcean, L.H. Delmau, B.A. Moyer, J.L. Sessler, W.-.S. Cho, D. Gross, G.W. Bates, S.J. Brooks, M.E. Light, P.A. Gale, Calix[4]pyrrole: an old yet new ion-pair receptor, Angew. Chem. Int. Ed. 44 (2005) 2537–2542, doi:10.1002/anie.200462945.
[10] M. Ciardi, F. Tancini, G. Gil-Ramírez, E.C. Escudero Adán, C. Massera, E. Dalcanale, P. Ballester, Switching from separated to contact ion-pair binding modes with diastereomeric Calix[4]pyrrole bis-phosphonate receptors, J. Am. Chem. Soc. 134 (2012) 13121–13132, doi:10.1021/ja305684m.
[11] S. Yuvayapan, A. Aydogan, Counter cation dependent and stimuli responsive supramolecular polymers constructed by calix[4]pyrrole based host–guest interactions, Eur. J. Org. Chem. 2019 (2019) 633–639, doi:10.1002/ejoc.201801663.
[12] P.A. Gale, J.L. Sessler, V. Král, V. Lynch, Calix[4]pyrroles: old yet new anion-binding agents, J. Am. Chem. Soc. 118 (1996) 5140–5141. https://doi.org/10.1021/ja960307r.
[13] M.-C. Husson, M. Schiff, A. Fouilhoux, A. Cano, D. Dobbelaere, A. Brassier, K. Mention, J.-B. Arnoux, F. Feillet, B. Chabrol, N. Guffon, C. Elie, P. de Lonlay, Efficacy and safety of i.v. sodium benzoate in urea cycle disorders: a multicentre retrospective study, Orphanet J. Rare Dis. 11 (2016) 127, doi:10.1186/s13023-016-0513-0.
[14] J.R. Blas, J.M. López-Bes, M. Márquez, J.L. Sessler, F.J. Luque, M. Orozco, Exploring the dynamics of calix[4]pyrrole: effect of solvent and fluorine substitution, Chem. Eur. J. 13 (2007) 1108–1116, doi:10.1002/chem.200600757.
[15] P. Anzenbacher Jr., A.C. Try, H. Miyaji, K. Jursíková, V.M. Lynch, M. Marquez, J.L. Sessler, Fluorinated calix[4]pyrrole and dipyrrolylquinoxaline: neutral anion receptors with augmented affinities and enhanced selectivities, J. Am. Chem. Soc. 122 (2000) 10268–10272, doi:10.1021/ja002112w.
[16] J.L. Sessler, W.-S. Cho, D.E. Gross, J.A. Shriver, V.M. Lynch, M. Marquez, Anion binding studies of fluorinated expanded calixpyrroles, J. Org. Chem. 70 (2005) 5982–5986, doi:10.1021/jo050662c.
[17] G. Cafeo, F.H. Kohnke, A.J.P. White, D. Garozzo, A. Messina, Syntheses, structures, and anion-binding properties of two novel calix[2]benzo[4]pyrroles, Chem. Eur. J. 13 (2007) 649–656, doi:10.1002/chem.200600452.
[18] W. Sato, H. Miyaji, J.L. Sessler, Calix[4]pyrrole dimers bearing rigid spacers: towards the synthesis of cooperative anion binding agents, Tetrahedron Lett. 41 (2000) 6731–6736, doi:10.1016/S0040-4039(00)01105-9.
[19] P. Anzenbacher, K. Jursíková, V.M. Lynch, P.A. Gale, J.L. Sessler, Calix[4]pyrroles containing deep cavities and fixed walls. Synthesis, structural studies, and anion binding properties of the isomeric products derived from the condensation of *p*-hydroxyacetophenone and pyrrole, J. Am. Chem. Soc. 121 (1999) 11020–11021, doi:10.1021/ja993195n.
[20] B. Verdejo, G. Gil-Ramírez, P. Ballester, Molecular recognition of pyridine N-oxides in water using calix[4]pyrrole receptors, J. Am. Chem. Soc. 131 (2009) 3178–3179, doi:10.1021/ja900151u.
[21] G. Moncelsi, L. Escobar, H. Dube, P. Ballester, 2-(4′-Pyridyl-N-oxide)-substituted hemithioindigos as photoresponsive guests for a super aryl-extended Calix[4]pyrrole receptor, Chem. Asian J. 13 (2018) 1632–1639, doi:10.1002/asia.201800463.
[22] L. Bonomo, E. Solari, G. Toraman, R. Scopelliti, C. Floriani, M. Latronico, A cylindrical cavity with two different hydrogen-binding boundaries: the calix[4]arene skeleton screwed onto the *meso*-positions of the calix[4]pyrrole, Chem. Commun. 140 (1999) 2413–2414, doi:10.1039/a907563a.
[23] C. Guo, H. Wang, V.M. Lynch, X. Ji, Z.A. Page, J.L. Sessler, Molecular recognition of pyrazine N,N′-dioxide using aryl extended calix[4]pyrroles, Chem. Sci. 11 (2020) 5650–5657, doi:10.1039/d0sc01496f.
[24] L. Adriaenssens, C. Estarellas, A. Vargas Jentzsch, M. Martinez Belmonte, S. Matile, P. Ballester, Quantification of nitrate-π interactions and selective transport of nitrate using Calix[4]pyrroles with two aromatic walls, J. Am. Chem. Soc. 135 (2013) 8324–8330, doi:10.1021/ja4021793.
[25] A. Kim, R. Ali, S.H. Park, Y.-H. Kim, J.S. Park, Probing and evaluating anion-π interaction in meso-dinitrophenyl functionalized calix[4]pyrrole isomers, Chem. Commun. 52 (2016) 11139–11142, doi:10.1039/c6cc04562f.
[26] C.R. Groom, I.J. Bruno, M.P. Lightfoot, S.C. Ward, The Cambridge structural database, Acta Crystallogr. Sect. B. 72 (2016) 171–179, doi:10.1107/S2052520616003954.
[27] Y.-C. He, J.-G. Pan, D.-S. Liu, CCDC 1443141: Experimental crystal structure determination, Exp. Cryst. Struct. Determ. (2016), doi:10.5517/ccdc.csd.cc1kfpym.
[28] B. Verdejo, F. Rodríguez-Llansola, B. Escuder, J.F. Miravet, P. Ballester, Sodium and pH responsive hydrogel formation by the supramolecular system calix[4]pyrrole derivative/tetramethylammonium cation, Chem. Commun. 47 (2011) 2017–2019, doi:10.1039/c0cc04051g.
[29] C. Caltagirone, N.L. Bill, D.E. Gross, M.E. Light, J.L. Sessler, P.A. Gale, Bis-cation salt complexation by meso-octamethylcalix[4]pyrrole: linking complexes in solution and in the solid state, Org. Biomol. Chem. 8 (2010) 96–99, doi:10.1039/b916113a.
[30] J. Lee, J.T. Brewster, B. Song, V.M. Lynch, I. Hwang, X. Li, J.L. Sessler, Uranyl dication mediated photoswitching of a calix[4]pyrrole-based metal coordination cage, Chem. Commun. 54 (2018) 9422–9425, doi:10.1039/c8cc05160g.
[31] C. Frassineti, S. Ghelli, P. Gans, A. Sabatini, M.S. Moruzzi, A. Vacca, Nuclear magnetic resonance as a tool for determining protonation constants of natural polyprotic bases in solution, Anal. Biochem. 231 (1995) 374–382, doi:10.1006/abio.1995.9984.
[32] O.V. Dolomanov, L.J. Bourhis, R.J. Gildea, J.A.K. Howard, H. Puschmann, OLEX2 : a complete structure solution, refinement and analysis program, J. Appl. Cryst. 42 (2009) 339–341, doi:10.1107/S0021889808042726.
[33] G.M. Sheldrick, SHELXT - Integrated space-group and crystal-structure determination, Acta Crystallogr. Sect. A 71 (2015) 3–8, doi:10.1107/S2053273314026370.
[34] L. Palatinus, G. Chapuis, SUPERFLIP - A computer program for the solution of crystal structures by charge flipping in arbitrary dimensions, J. Appl. Crystallogr. 40 (2007) 786–790, doi:10.1107/S0021889807029238.
[35] L. Palatinus, A. van der Lee, Symmetry determination following structure solution in P1, J. Appl. Crystallogr. 41 (2008) 975–984, doi:10.1107/S0021889808028185.
[36] L. Palatinus, S.J. Prathapa, S. van Smaalen, EDMA: a computer program for topological analysis of discrete electron densities, J. Appl. Crystallogr. 45 (2012) 575–580, doi:10.1107/S0021889812016068.

[37] G.M. Sheldrick, Crystal structure refinement with SHELXL, Acta Crystallogr. Sect. C 71 (2015) 3–8, doi:10.1107/S2053229614024218.
[38] M.J. Frisch, G.W. Trucks, H.B. Schlegel, G.E. Scuseria, M.A. Robb, J.R. Cheeseman, G. Scalmani, V. Barone, B. Mennucci, G.A. Petersson, H. Nakatsuji, M. Caricato, X. Li, H.P. Hratchian, A.F. Izmaylov, J. Bloino, G. Zheng, J.L. Sonnenberg, M. Hada, M. Ehara, K. Toyota, R. Fukuda, J. Hasegawa, M. Ishida, T. Nakajima, Y. Honda, O. Kitao, H. Nakai, T. Vreven, J.A. Montgomery Jr., J.E. Peralta, F. Ogliaro, M. Bearpark, J.J. Heyd, E. Brothers, K.N. Kudin, V.N. Staroverov, T. Keith, R. Kobayashi, J. Normand, K. Raghavachari, A. Rendell, J.C. Burant, S.S. Iyengar, J. Tomasi, M. Cossi, N. Rega, J.M. Millam, M. Klene, J.E. Knox, J.B. Cross, V. Bakken, C. Adamo, J. Jaramillo, R. Comperts, R.E. Stratmann, O. Yazyev, A.J. Austin, R. Cammi, C. Pomelli, J.W. Ochterski, R.L. Martin, K. Morokuma, V.G. Zakrzewski, G.A. Voth, P. Salvador, J.J. Dannenberg, S. Dapprich, A.D. Daniels, O. Farkas, J.B. Foresman, J.V. Ortiz, J. Cioslowski, D.J. Fox, Gaussian 09, Revision E.01, Gaussian, Inc., Wallingford CT, 2013.
[39] A.D. Becke, Density-functional thermochemistry. III. The role of exact exchange, J. Chem. Phys. 98 (1993) 5648–5652, doi:10.1063/1.464913.
[40] P.J. Stephens, F.J. Devlin, C.F. Chabalowski, M.J. Frisch, Ab Initio calculation of vibrational absorption and circular dichroism spectra using density functional force fields, J. Phys. Chem. 98 (1994) 11623–11627, doi:10.1021/j100096a001.
[41] R. Krishnan, J.S. Binkley, R. Seeger, J.A. Pople, Self-consistent molecular orbital methods. XX. A basis set for correlated wave functions, J. Chem. Phys. 72 (1980) 650–654, doi:10.1063/1.438955.
[42] M.M. Francl, W.J. Pietro, W.J. Hehre, J.S. Binkley, M.S. Gordon, D.J. DeFrees, J.A. Pople, Self-consistent molecular orbital methods. XXIII. A polarization-type basis set for second-row elements, J. Chem. Phys. 77 (1982) 3654–3665, doi:10.1063/1.444267.
[43] A.D. McLean, G.S. Chandler, Contracted Gaussian basis sets for molecular calculations. I. Second row atoms, Z=11–18, J. Chem. Phys. 72 (1980) 5639–5648, doi:10.1063/1.438980.
[44] G.W. Spitznagel, T. Clark, P. von Ragué Schleyer, W.J. Hehre, An evaluation of the performance of diffuse function-augmented basis sets for second row elements, Na-Cl, J. Comput. Chem. 8 (1987) 1109–1116, doi:10.1002/jcc.540080807.
[45] S. Grimme, J. Antony, S. Ehrlich, H. Krieg, A consistent and accurate ab initio parametrization of density functional dispersion correction (DFT-D) for the 94 elements H-Pu, J. Chem. Phys. 132 (2010) 154104, doi:10.1063/1.3382344.
[46] Schrödinger Release 2020-4: Maestro Version 12.6.144, Schrödinger, LLC, New York, NY, 2020.
[47] C.F. Macrae, I. Sovago, S.J. Cottrell, P.T.A. Galek, P. McCabe, E. Pidcock, M. Platings, G.P. Shields, J.S. Stevens, M. Towler, P.A. Wood, Mercury 4.0: from visualization to analysis, design and prediction, J. Appl. Crystallogr. 53 (2020) 226–235, doi:10.1107/S1600576719014092.
[48] G. Cafeo, F.H. Kohnke, L. Valenti, A.J.P. White, pH-controlled molecular switches and the substrate-directed self-assembly of molecular capsules with a calix[4]pyrrole derivative, Chem. Eur. J. 14 (2008) 11593–11600, doi:10.1002/chem.200800819.
[49] R. Molina-Muriel, G. Aragay, E.C. Escudero-Adán, P. Ballester, Switching from negative-cooperativity to no-cooperativity in the binding of ion-pair dimers by a bis(calix[4]pyrrole) macrocycle, J. Org. Chem. 83 (2018) 13507–13514, doi:10.1021/acs.joc.8b02449.
[50] P. Ballester, G. Gil-Ramírez, Self-assembly of dimeric tetraurea calix[4]pyrrole capsules, PNAS 106 (2009) 10455–10459, doi:10.1073/pnas.0809612106.
[51] V. Valderrey, E.C. Escudero-Adán, P. Ballester, Polyatomic anion assistance in the assembly of [2]pseudorotaxanes, J. Am. Chem. Soc. 134 (2012) 10733–10736, doi:10.1021/ja301900s.
[52] L. Adriaenssens, G. Gil-Ramírez, A. Frontera, D. Quiñonero, E.C. Escudero-Adán, P. Ballester, Thermodynamic characterization of halide-π interactions in solution using “two-wall” aryl extended calix[4]pyrroles as model system, J. Am. Chem. Soc. 136 (2014) 3208–3218, doi:10.1021/ja412098v.
[53] T. Hirao, D.S. Kim, X. Chi, V.M. Lynch, K. Ohara, J.S. Park, K. Yamaguchi, J.L. Sessler, Control over multiple molecular states with directional changes driven by molecular recognition, Nat. Commun. 9 (2018) 823, doi:10.1038/s41467-018-03220-0.